On-Body Long-Range Wireless Backscattering Sensing System Using Inkjet-/3-D-Printed Flexible Ambient RF Energy Harvesters Capable of Simultaneous DC and Harmonics Generation

Tong-Hong Lin, Jo Bito, *Student Member, IEEE*, Jimmy G. D. Hester, *Member, IEEE*, John Kimionis, *Member, IEEE*, Ryan A. Bahr, *Graduate Student Member, IEEE*, and Manos M. Tentzeris, *Fellow, IEEE*

***Abstract*— A novel wearable and flexible energy autonomous on-body sensing network is proposed featuring full operability through energy harvesting from a hand-held 464.5-MHz UHF two-way talk radio. Three different functions are provided utilizing the hand-held two-way talk radio as the only energy source for our proposed system. There are two types of energy harvesters (EHs) proposed for the presented system. The first EH that is mounted on the sensing capable backscattering RFID tags harvests the 464.5-MHz signal energy to drive the tags; the second EH that can be worn on hands harvests the same 464.5-MHz signal to produce both the dc power and the carrier signal. The second EH is more efficient than conventional ambient RF energy harvesting architectures because for the first time, both the dc and the second harmonics generated by the rectifier are utilized to enable two additional functions. The generated second harmonic is used to interrogate backscattering RFID tags for on-body sensing, while the dc power is used to power an RF amplifier in order to enhance the second harmonic to effectively extend the sensing and communication range. For the proof-of-concept demonstration, the measured dc and the second harmonic, 929 MHz, output power from the proposed EH are 17.5 and 1.43 dBm, respectively, while a two-way talk radio is 9 cm away. The measured second harmonic output power is increased to 13 dBm utilizing the harvester-powered RF amplifier, and the reading range of the custom backscattering sensor tag is extended to more than 70 m. Also, the interrogation of multiple sensor tags and the wireless detection of ammonia gas utilizing an inkjet printed flexible ammonia sensor are demonstrated showing the wide range of applications of the proposed approach.**

***Index Terms*— Backscatter sensors, energy harvesting, flexible, inkjet printing, on-body sensing network, RFID, smart skin, 3-D printing, wearable.**

Manuscript received July 1, 2017; revised October 3, 2017; accepted October 12, 2017. Date of publication November 21, 2017; date of current version December 12, 2017. This work was supported in part by the Packaging Research Center, Georgia Institute of Technology, in part by the National Science Foundation Emerging Frontiers in Research and Innovation, in part by the Defense Threat Reduction Agency, in part by the Semiconductor Research Corporation, and in part by Texas Instruments Incorporated. This paper is an expanded version from the 2017 IEEE MTT-S International Microwave Symposium Conference, Honolulu, HI, USA, June 4–9, 2017. *(Corresponding author: Tong-Hong Lin.)*

The authors are with the School of Electrical and Computer Engineering, Georgia Institute of Technology, Atlanta, GA 30332-250 USA (e-mail: tlin97@gatech.edu).

Color versions of one or more of the figures in this paper are available online at http://ieeexplore.ieee.org.

Digital Object Identifier 10.1109/TMTT.2017.2768033

I. Introduction

THE idea of applying Internet of Things (IoT) and wireless sensor networks (WSNs) to build smart cities and smart skins has become extremely popular in the last decade [1], [2]. These technologies expect to deploy hundreds or even thousands of sensors in the cities or on the clothes and collect multiply sensing data to analyze and monitor the security of the cities or the health status in real time. However, conventional sensor devices are mostly relying primarily on batteries, which require replacement after at most few years of operation. Due to the large number of sensors, it is nearly impossible to change the batteries of the sensor nodes one by one because of the excessive cost. Hence, one of the biggest challenges is to realize energy autonomous sensing systems eliminating the use of conventional batteries.

Ambient energy harvesting is a good solution to power these sensing devices by harnessing ambient energy from existing ambient energy sources such as solar, heat, and vibration. Among all sources, RF energy sources are popular since they can be accessed all day while their inherent ability of bypassing or penetrating walls makes them ubiquitously available. There are many different types of RF energy sources, such as UHF communication, WiFi, and digital TV signals, especially in urban environments [3], [4]. The challenges associated with the relatively low energy density of ambient RF energy sources [5] have been commonly addressed using high gain antennas and broadband or multiband antennas [3], [6], [7] for low energy far-field RF energy harvesting applications. However, in addition to those RF energy sources with relatively low energy density, there are numerous "hotspots" where RF energy is fairly high, which can generate very high dc voltage and power and alleviate the issues of low energy density and ICs' "cold start" [8]. As an example, wearable energy harvesters (EHs) for two-ways talk radio, which is a typical communication device, have been reported and used as the energy source of a microcontroller unit (MCU) for wireless sensing [9].

In most of previously reported ambient RF EHs in literature, the main focus of harvester design is to maximize the output

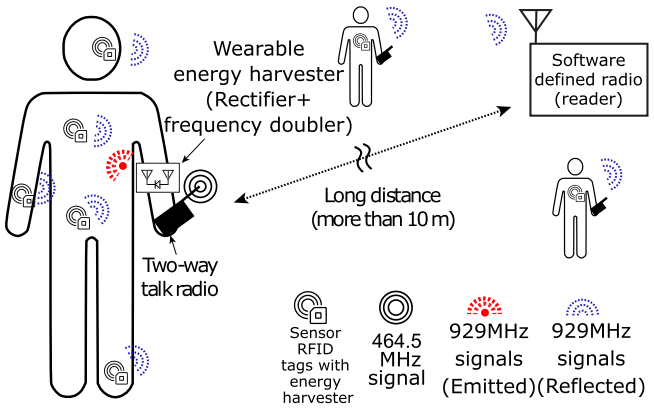

Fig. 1. Proposed wearable energy-autonomous on-body WSN system.

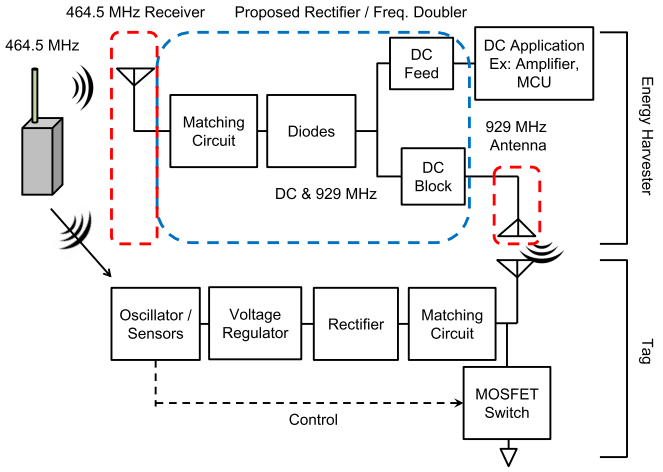

Fig. 2. Block diagram of the proposed system.

dc power [10]–[12]. Therefore, output filters are used in the designs of typical energy harvesting circuits to eliminate harmonics created during rectification. However, for wireless sensing applications, wireless communication of sensing data is another important aspect in the system and these commonly wasted harmonics can be utilized for communication. The conventional approach for wireless communication is to utilize a transceiver IC and to transmit the sensing data obtained by utilizing analog to digital converters, but this approach requires power hungry dc-RF conversion and RF signal amplification processes and is not suitable for ambient RF energy harvesting, which has limited power supply [13]. Another approach is to utilize conventional passive RFID and backscattering for sensing, but the reading range of conventional RFID sensor networks is about only 3 m [1]. The reading range is so small that multiple RFID readers need to be arranged to collect the data, resulting in a dramatically increased implementation cost. Thus, another key challenge is to significantly increase the reading range of the RFID sensor tags. To extend the reading range of the passive RFID tags, it has been proven that multiple carrier emitters can be used to illuminate nearby RFIDs in bistatic RFID reader configurations [14]. However, these carrier emitters are not energy autonomous which means there is additional maintenance cost. Moreover, especially for smart skin applications, the sensors worn on users change their location following body movements. Thus, carrier emitters with fixed positions might not be able to cover them all the time and mobile/protable carrier emitters are necessary. Since the two-way talk radio is utilizing analog modulated signals [9], harmonics from the EH include continuous RF signals, which can be used to realize a carrier emitter for passive RFIDs.

In this paper, a novel wearable energy-autonomous on-body WSN system is proposed as depicted in Fig. 1. To realize this system, a wearable and flexible EH which harnesses near-field energy from a 464.5-MHz two-way talk radio is proposed using inkjet and 3-D printing techniques for its fabrication. In the proposed EH circuit, both dc power and the second harmonic at 929 MHz are utilized for different applications. The RF second harmonic signal output can be used as a wearable mobile carrier emitter to simultaneously illuminate multiple on-body sensing capable backscattering RFID tags and extend their reading ranges. Meanwhile, the dc power output can be used to drive an RF amplifier to further extend the operation range. Similarly, the oscillator in the tags are powered by an integrated EH harnessing the 464.5-MHz signals from the two-way talk radio. Thus, this EH is the first ever demonstration of an energy autonomous system which enables three different functions simultaneously to establish an on-body autonomous sensing network by utilizing a single ambient RF energy source. As an extended version of the previous work [15], further characterization of the proposed EH, integration printed ammonia sensors into backscattering tags as a practical IoT sensing application, and a further range extension by driving the RF amplifier with the dc power provided by the proposed EH along with more detailed field operation tests are demonstrated.

II. System Architecture

The detailed block diagram of the proposed system is shown in Fig. 2. The system is composed of one EH and multiple on-body sensing tags. The only energy source for the entire system is a 464.5-MHz two-way talk radio with the measured power spectrum shown in Fig. 3. The output powers are 34.3 and −29 dBm at 464.5 and 929 MHz, respectively.

The EH section is composed of three main components; a 464.5-MHz receiver, a proposed rectifier/frequency doubler, and a 929-MHz antenna. The 464.5-MHz near-field receiver is used to harness the power radiated from the radio, which is later sent to the rectifier/frequency doubler that generates the following outputs: the dc power is used to drive a dc device/IC/application and the RF output is fed to a 929-MHz antenna.

For the interrogated tag design, the 464.5-MHz signal that comes from the two-way radio is harvested by the integrated EH which is composed of a matching circuit, a rectifier circuit, and a voltage regulator. The harvested power is used to drive the oscillator. While the oscillator is properly driven by the rectifier, it is used to control the MOSFET switch to create the modulated backscattered signals using the 929-MHz signal generated by the energy harvesting circuit as the carrier.

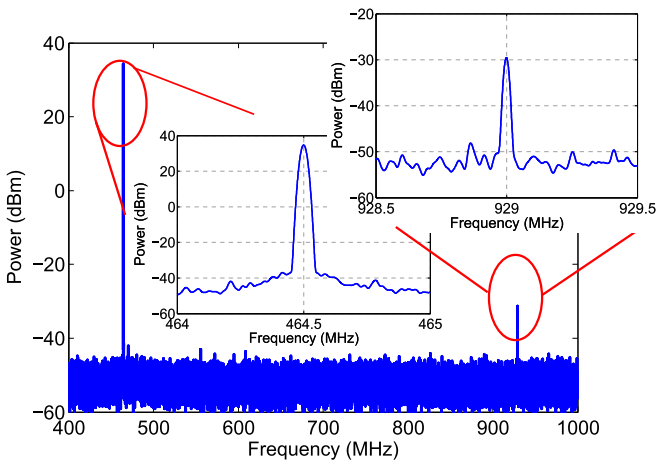

Fig. 3. Measured power spectrum of the off-the-shelf two-way talk radio.

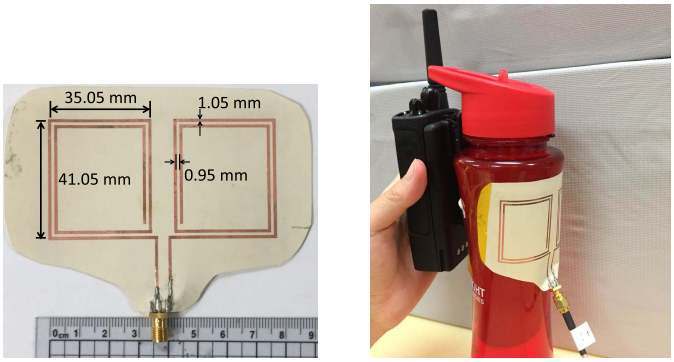

(a) (b)

Fig. 4. (a) Prototype of the 464.5-MHz antenna. (b) "On-body emulating" setup of the coupling test for the 464.5-MHz antenna.

In summary, the 464.5-MHz two-way talk radio is used as an energy source to serve three different purposes as follows:

1) to power RF amplifier IC as an dc application;
2) to create carrier emitter signals for the interrogated tag/sensor;
3) to power the oscillator IC in backscattering tags.

Besides, since the carrier emitter is wearable, mobile, and capable of moving with the user, the relative distances between the wearable RFID tags and the carrier emitter would not change dramatically. Thus, all wearable RFID tags are in the proximity of the carrier emitter all the time significantly enhancing their readability.

III. Energy Harvester Design and Characterization

A. Inkjet Printed 464.5-MHz Antenna Design

A proof-of-concept prototype of 464.5-MHz near-field receiver/antenna fabricated utilizing inkjet printing masking technique and its physical dimensions are shown in Fig. 4(a). This receiver is designed with an open-type helical coil structure to enhance coupling between the two-way talk radio and the 464.5-MHz receiver. The "on-body emulating" setup of the coupling test for this 464.5-MHz antenna is shown in Fig. 4(b). The distance between the two-way talk radio and the 464.5-MHz antenna is 9 cm. Moreover, the circuit is mounted on a water bottle filled with water to mimic the effects of the human body [9]. The dielectric constant and the conductivity of the water are 82 and 0.01 S/m, respectively. The 464.5-MHz antenna is connected to the spectrum analyzer to measure the received power level, which is found to be around 20 dBm. The power supply from the two-way talk radio is 36 dBm and about 2.5% of the power is harvested by the 464.5-MHz near-field coupling antenna. The harvested energy is large enough to drive all components but not too large to affect significantly the quality and performance of the overall communication.

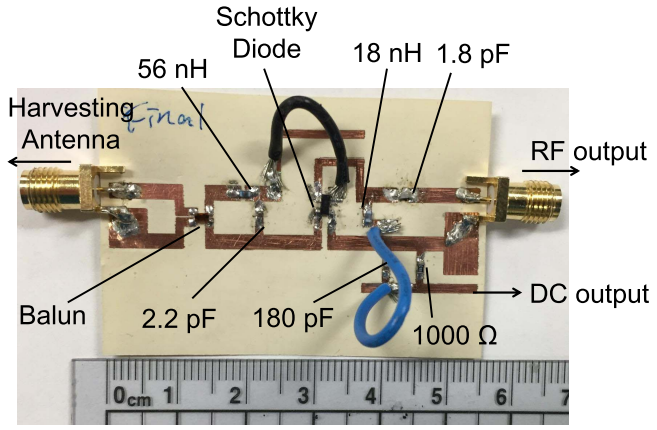

Fig. 5. Prototype of the proposed full-wave rectifier/frequency doubler.

B. Proposed Rectifier/Frequency Doubler

Since one of the most commonly used frequency bands for RFID tags is 860–960 MHz, the second harmonic of 929-MHz signals would be a good choice for the carrier emitter. Thus, the main goal of the proposed rectifier/frequency doubler is to generate as large power as possible at the dc and the second harmonic frequencies. Therefore, a full-wave rectifier topology, which can theoretically eliminate the odd-order harmonics, is adapted. Hence, the largest remaining harmonic is the second harmonic.

Fig. 5 shows a prototype of the proposed rectifier. A balun is used, as demonstrated in Fig. 5, to guarantee the differential feeding of the full-wave rectifier. The matching circuit is composed of a 56-nH series inductor and a 2.2-pF parallel capacitor. The HSMS 2828 Schottky diode package is used to perform the full-wave rectification. The 1.8-pF capacitor and the 18-nH inductor are serving as a dc block and a dc feed, respectively. Finally, a 180-pF capacitor is used to eliminate higher order harmonics while a 1-kΩ resistor acts as the load. This 1-kΩ resistor is chosen because the RF-dc conversion efficiency of the rectifier is the highest under this load value.

The measured dc and RF output power levels from the proposed rectifier with respect to the input power are shown in Fig. 6. The simulated results using Advanced Design System are also included for comparison. As shown in Fig. 6, good agreements between the simulated and measured results can be observed. The maximum RF-dc conversion efficiency is

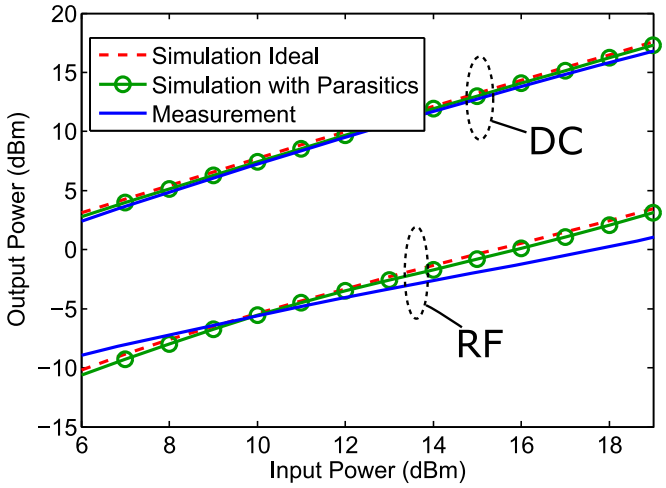

Fig. 6. Simulated and measured output dc and RF power levels from the proposed rectifier/frequency doubler with respect to the input power.

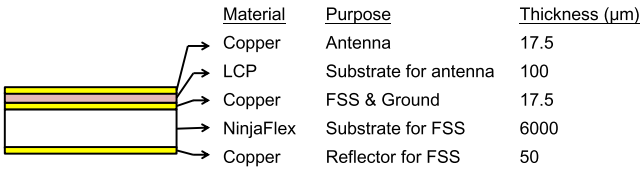

Material	Purpose	Thickness (μm)
Copper	Antenna	17.5
LCP	Substrate for antenna	100
Copper	FSS & Ground	17.5
NinjaFlex	Substrate for FSS	6000
Copper	Reflector for FSS	50

Fig. 7. Side view of the wearable 929-MHz antenna.

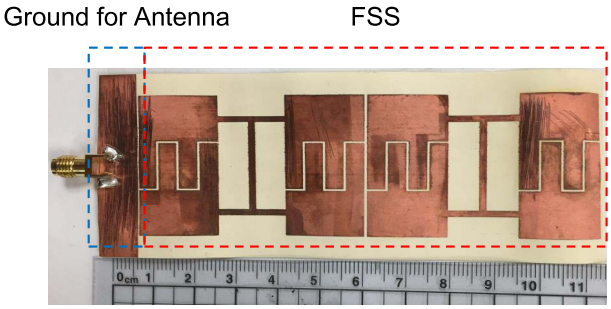

Fig. 8. Prototype of the FSS.

about 61% and the maximum RF (464.5–929 MHz) conversion efficiency is about 3.8%. The maximum total conversion efficiency is 63.1% when 19-dBm RF input power is provided. The maximum output dc and RF power levels are 17.27 and 1.41 dBm when the input power is about 19 dBm.

C. Inkjet and 3-D Printed 929-MHz Antenna Design

The 929-MHz antenna is a Z-shaped monopole antenna with an artificial magnetic conductor (AMC) on the back that is used to eliminate the effects of the human body on the antenna [16]. The side view of this antenna is shown in Fig. 7. It is composed of five layers. The top (copper) layer is used for the Z-shaped monopole antenna. The second layer is the LCP substrate. The AMC structure is composed of a frequency selective surface (FSS), a spacer, and a metal reflector which are corresponding to the third, fourth, and fifth layer, respectively. The thickness and the purpose of each layer

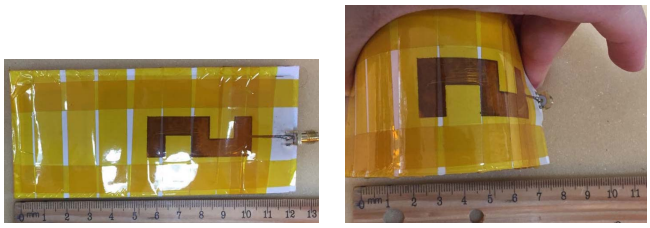

Fig. 9. Prototype of the (a) unfolded and (b) folded 929-MHz antenna.

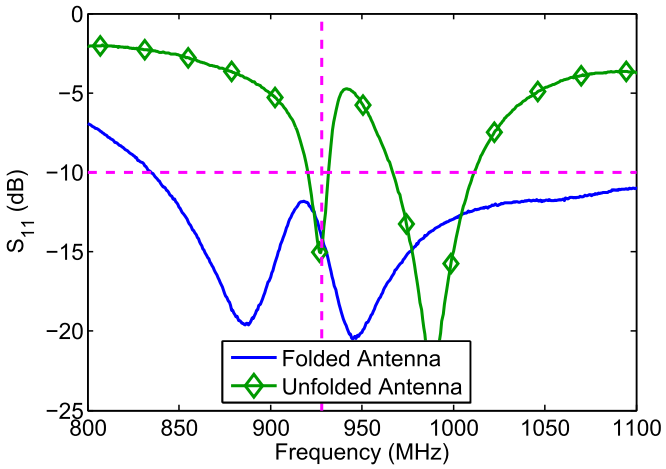

Fig. 10. Measured S_{11} of the folded and unfolded 929-MHz wearable antenna.

are also included in Fig. 7. The pattern of the FSS and the ground plane for the monopole are contained in the third layer as shown in Fig. 8.

The fourth layer is a spacer between the metal reflector and the FSS. The thickness of this layer is extremely important since it affects significantly the bandwidth and the operating frequency of the AMC plane [16]. However, the thickness of this layer cannot be designed arbitrarily if off-shelf substrates are used. The reason is that the thicknesses of off-shelf substrates are limited to specific discrete values and it is hard to realize substrates with custom/optimized thicknesses. The 3-D printing technique offers a good solution to this problem. The minimum and maximum thickness that can be realized using Printrbot Metal Plus 3-D printer are 127 μm and 25 cm, respectively. Thus, by 3-D printing flexible thermoplastic polyurethane NinjaFlex [17], almost any arbitrary thickness values can be realized and a more optimal design of the AMC plane can be achieved. The final layer is a reflector fabricated using copper tape. The prototype of the 929-MHz antenna is shown in Fig. 9(a). Furthermore, since the 929-MHz antenna is wearable and flexible, the prototype under the folded condition is also shown in Fig. 9(b) demonstrating a very good flexibility. The length of the unfolded one is about 12.5 cm and can be folded to about 8 cm. The measured scattering parameter values of the wearable 929-MHz antenna are shown in Fig. 10. Measured results for the folded and the unfolded conditions are included. As demonstrated in Fig. 10, the return loss values at 929 MHz for folded and unfolded conditions are 14.1 and 14.8 dB, respectively.

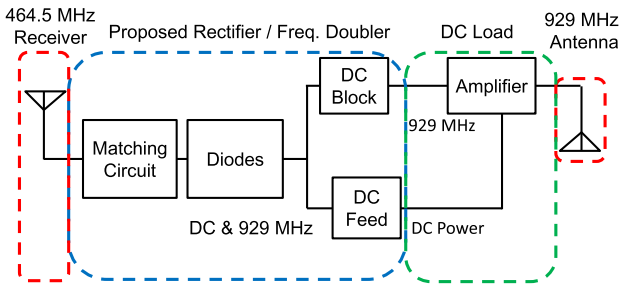

Fig. 11. Block diagram of the proposed EH with enhanced RF output by driving an RF amplifier using dc output power.

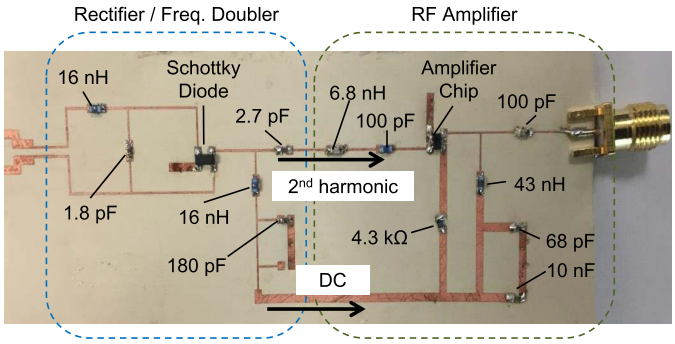

Fig. 12. Proof-of-concept prototype of the proposed rectifier/frequency doubler including a dc power enabled amplifier.

IV. Multiple Uses of Harvester DC Output Power

Two different output power, dc and 929-MHz continuous RF power, are provided by the proposed EH. The 929-MHz RF output signal is utilized to create a carrier emitter to enhance the reading range of the wearable passive RFID tags. In the previously reported results in [15], 1-kΩ resister was utilized and the dc power was not fully utilized. The dc power generated here is a convenient source to drive different applications since the voltage and the power are both high enough to drive most low power applications immediately without requiring a waiting time for charging. There are two potential categories of uses for the dc power. The first one is to achieve a function which is uncorrelated with the carrier emitter. For example, the dc power can be used to drive an RFID reader chip, thus enabling a wearable reader. The other one is to be appropriately combined with the RF power to achieve more complex functions or further range extension. For example, the dc power can be used to drive an MCU to achieve modulated carrier emitter signals or drive an RF amplifier to enhance the carrier emitter power thus leading to a further range extension.

In this research, the RF amplifier IC was added as a dc-power enabled component to increase the 929-MHz RF output power level extending the range of backscattering communication and sensing. The new block diagram of the proposed EH with the amplifier is depicted in Fig. 11 with a proof-of-concept prototype shown in Fig. 12. The difference between the prototype shown in Figs. 5 and 12 is that the dc load in Fig. 5 is a resistance which is replaced by an amplifier in Fig. 12. As shown in Fig. 12, the matching circuit

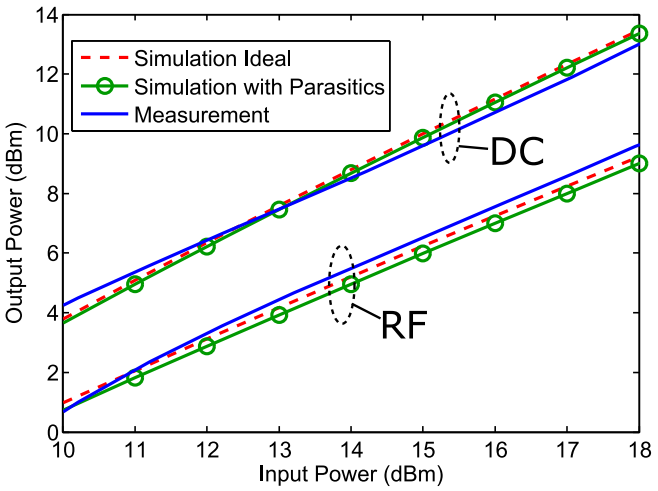

Fig. 13. Simulated and measured output dc and RF power levels from the proposed rectifier/frequency doubler with an RF amplifier (Fig. 12).

is composed of a 16-nH series inductor and a 1.8-pF parallel capacitor. The HSMS 2828 Schottky packaged diode is used to perform the full-wave rectification. The 2.7-pF capacitor and the 16-nH inductor are serving as a dc block and a dc feed, respectively. A 180-pF capacitor is used to eliminate higher order harmonics. The 929-MHz signal is then fed to the input matching circuit of the amplifier which is composed of a series 6.8-nH inductor and a series 100-pF capacitor and then fed to the input pin of the MGA-68563 RF amplifier chip. On the other hand, the dc power is connected to the amplifier bias circuit which is composed of a 4.3-kΩ resistor, a 10-nF capacitor, a 68-pF capacitor, and a 43-nH inductor.

The measured dc and RF output levels from the proposed rectifier including an RF amplifier with respect to the input power are shown in Fig. 13. The simulated results are also included for comparison and a good agreement between the simulated and measured results can be observed. As shown in Fig. 13, the maximum RF-dc conversion efficiency is about 33% and the maximum RF(464.5 MHz)–RF(929 MHz) conversion efficiency is about 14.8%, thus leading to the maximum total efficiency of 47.8% when 19-dBm RF input power is provided. The RF-dc conversion efficiency is smaller compared to Fig. 6 (61%). The reason is that the resistance used in Fig. 6 is 1 kΩ which is much larger than the dc resistance of the RF amplifier which is about 0.2 kΩ [9]. Although the dc power is smaller, it can be still used to successfully drive the RF amplifier. Moreover, the comparison of the 929-MHz output between the harvesters with and without the amplifier is shown in Fig. 14. The output 929-MHz power is much larger with the help of the amplifier and the effect is more significant when the input power is larger. The 929-MHz output power is about 9 dB larger when the input 464.5-MHz signal is about 19 dBm. Since the carrier emitter is much stronger, a significantly enhanced interrogation range is expected. Furthermore, as shown in Fig. 3 the second harmonic noise generated by the two way radio is only −29 dBm. Thus, much larger carrier signal can be provided utilizing our proposed EH.

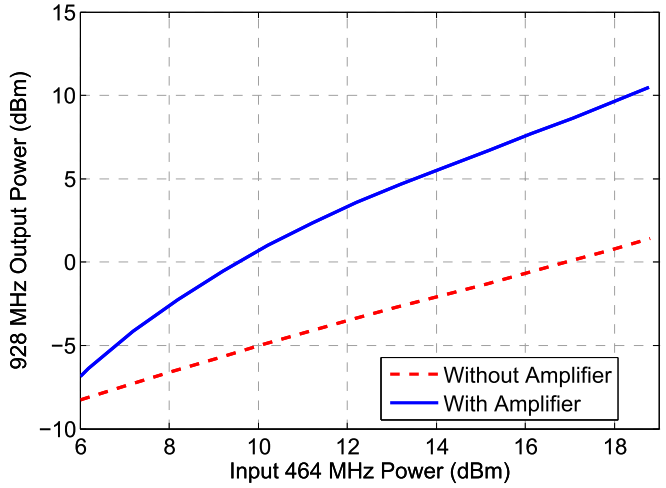

Fig. 14. Comparison of the 929-MHz output power between the harvesters with and without an RF amplifier.

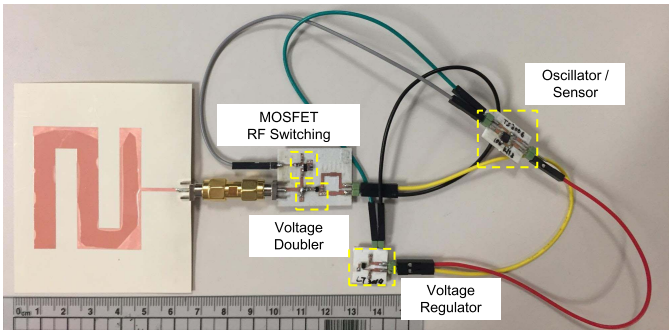

Fig. 15. Prototype of the custom-made backscattering RFID tag.

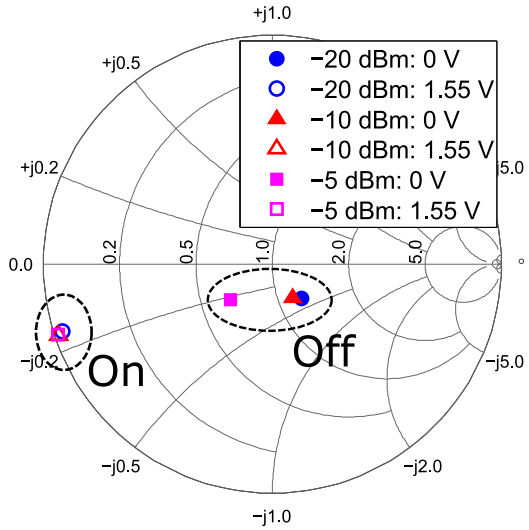

Fig. 16. Measured *S*-parameters of 929 MHz with each expected input power and MOSFET bias voltage.

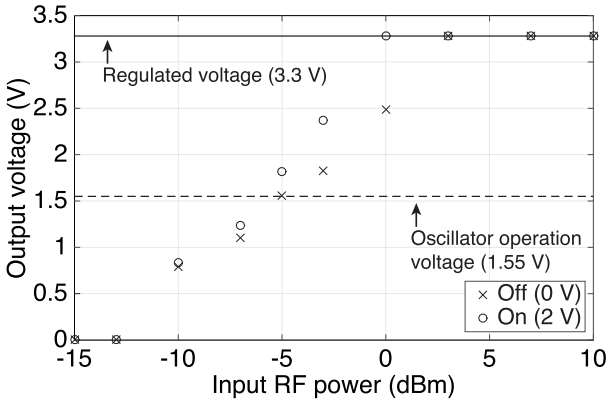

Fig. 17. Measured output voltage from the voltage regulator connected with the voltage doubler with 464.5-MHz RF input signal at each input power and MOSFET bias voltage.

V. Backscattering Sensor Tag Design

A. Backscattering Tag Design

For on-body communication and sensing applications, a custom backscatter tag was designed and fabricated as depicted in Fig. 15. The power received by the Z-shaped antenna of the tag is rectified by the voltage doubler. Then a 3.3-V voltage regulator (Linear technology LT3009) is connected between the voltage doubler and the oscillator to protect the oscillator. The output signal from the Silicon Labs TS3006 oscillator is applied to trigger an RF switching MOSFET (NXP BF1118) to create modulated backscattered signals. The design was based on the MOSFET front-end from [18], used in cutoff and saturation region. The modulation frequency varies depending on the impedance value of the sensing element connected to the oscillator thus enabling wireless sensing [19].

The 929-MHz signal is used as the carrier by the custom-made backscattering tag to send the modulated signals. Performing measurements utilizing a VNA, the input impedance of each input power level of 929-MHz signal (−5, −10, and −20 dBm) and MOSFET bias voltage condition (0 and 1.55 V) is obtained as depicted in Fig. 16. These bias condition are chosen because the MOSFET is "OFF" when the bias condition is 0 V and "ON" when the bias condition is 1.55 V. As shown in Fig. 16, the impedance values while the MOSFET is ON and OFF are very different. Hence, they can be used to binary modulate bits with the values "0" and "1." At 929 MHz for −20 dBm of RF input power, the difference in the magnitude of the normalized input impedance between 0- and 1.55-V bias voltage conditions is 0.775 and the phase difference is 112.3° as shown in the measurements.

The 464.5-MHz signal which comes from the two-way radio is harvested and used to drive the oscillator. Fig. 17 depicts the measured output voltage from the voltage regulator that is connected to the voltage doubler with respect to RF input power level (464.5 MHz) at each MOSFET bias voltage condition when a 824-kΩ resistor, which is the expected equivalent dc resistance of the oscillator IC, is connected as a load. According to the measured results, the tag requires about −5 dBm of input power to achieve 1.55 V to turn ON the operation of the oscillator IC.

The operation goals of the tag antenna are to harvest 464.5-MHz power from the hand-held two-way radio and backscatter the modulated signal to reader. However, a dual-band antenna is not suitable for wearable design due to its

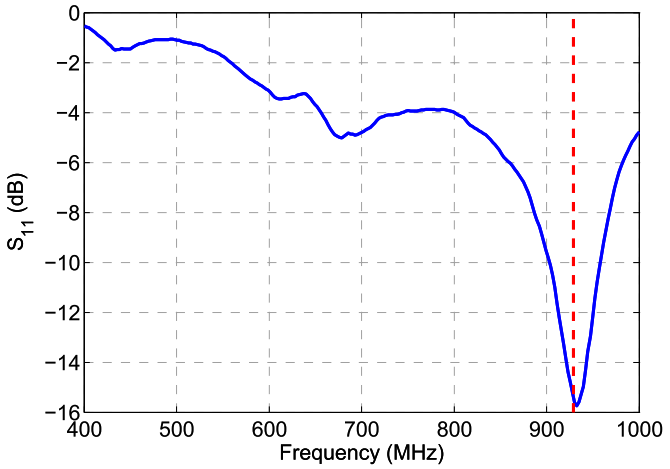

Fig. 18. Measured S_{11} of the 929-MHz antenna.

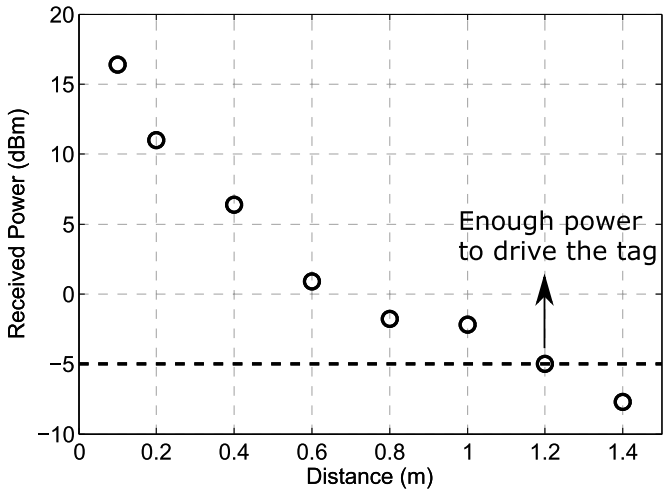

Fig. 19. Received 464.5-MHz power from the hand-held two-way radio by the tag antenna.

large size. Since only a small amount of power is required to drive the tag, an antenna which is operated at 929 MHz is sufficient because of the high transmitted power from the two-way talk radio. The measured S_{11} of the proof-of-concept antenna prototype is shown in Fig. 18 and a good matching at 929 MHz can be observed. The received 464.5-MHz power level using the Z-shaped antenna of the tag is shown in Fig. 19. The tag operation/interrogation range is about 1.2 m, which can cover the entire human body. Thus, even when the S_{11} at 464.5 MHz is only about -1.5 dB, the received power is large enough to drive the oscillator. This demonstrates the inherent flexibility of the proposed tag to operate effectively using practical on-body antennas without the need for high gain and large form-factors.

B. Integration With Ammonia Sensor

The modulation frequency is determined by the oscillation frequency which varies as a function of the external load resistance value of the oscillator IC. Therefore, it is possible to integrate arbitrary sensors (in this case a gas sensor) that

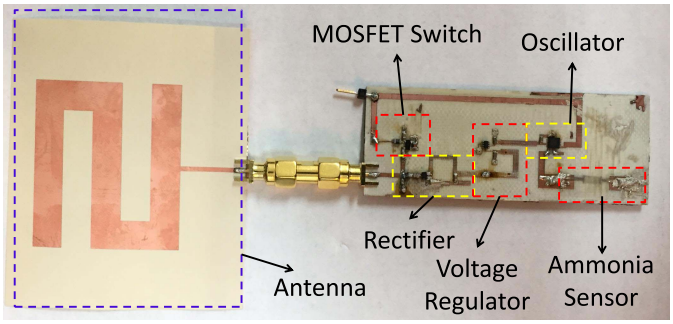

Fig. 20. Prototype of the custom backscattering RFID tag with a printed ammonia sensor.

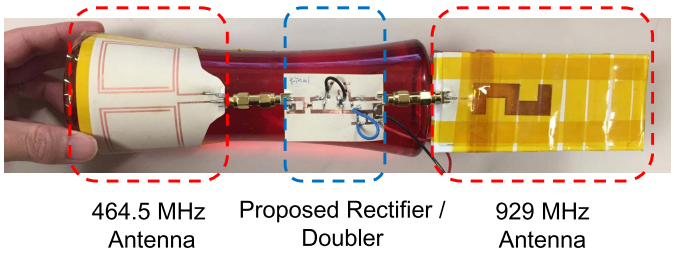

Fig. 21. Prototype of the energy harvesting circuit without an RF amplifier.

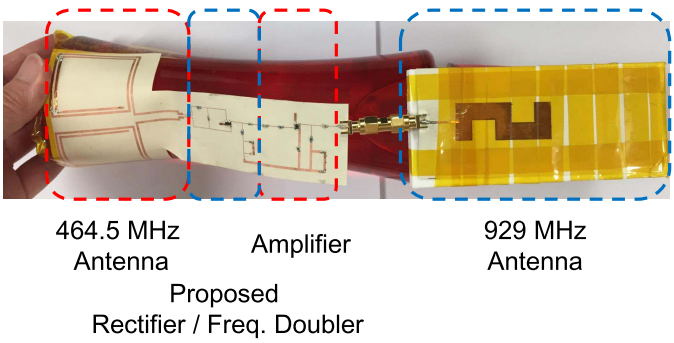

Fig. 22. Prototype of the energy harvesting circuit with an RF amplifier.

changes its impedance when it is exposed to certain chemicals, into the custom backscattering tag of Section V-A to detect the existence of specific gases by measuring the change in oscillation frequency. Therefore, the resistor in the previous prototype shown in Fig. 15 was replaced with a printed anmonnia sensor reported in [20] as depicted in Fig. 20. The impedance of the ammonia sensor increases when it is exposed to ammonia gas and the oscillation frequency is expected to decrease due to the change of the impedance. Experimental results shown in Section VI-C confirm this assumption.

VI. Performance Evaluation

A. Sensing and Backscattering Communication Range

The prototypes of the proposed EH without and with an RF amplifier are shown in Figs. 21 and 22, respectively. To evaluate the performance and the link budget of the proposed EH and the tag configuration, the ambient RF source (two-way talk radio) is placed at a distance of 9 cm from the proposed EH and the antenna of the tag is put 30 cm

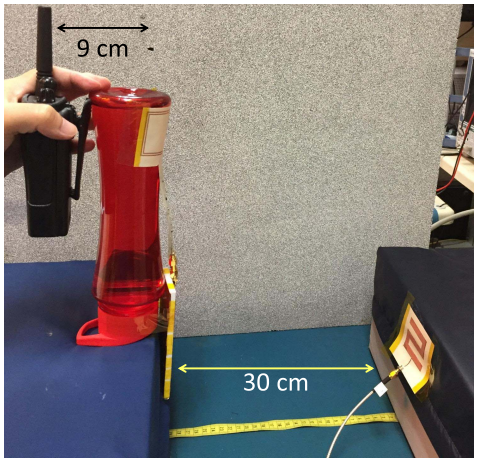

Fig. 23. Experimental setup for the testing of the link budget.

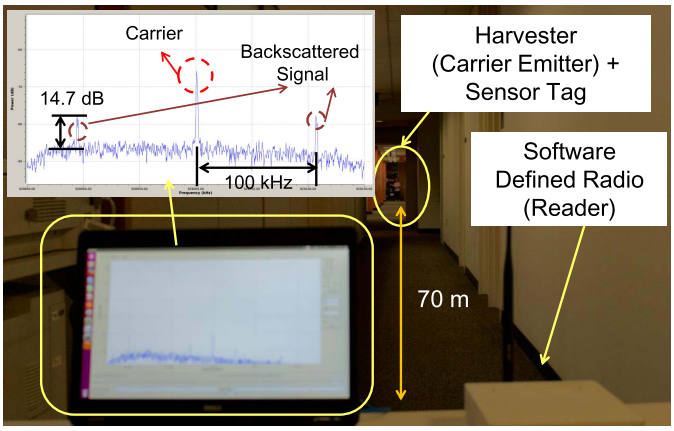

Fig. 24. Measurement setup for the long range on-body wireless sensing.

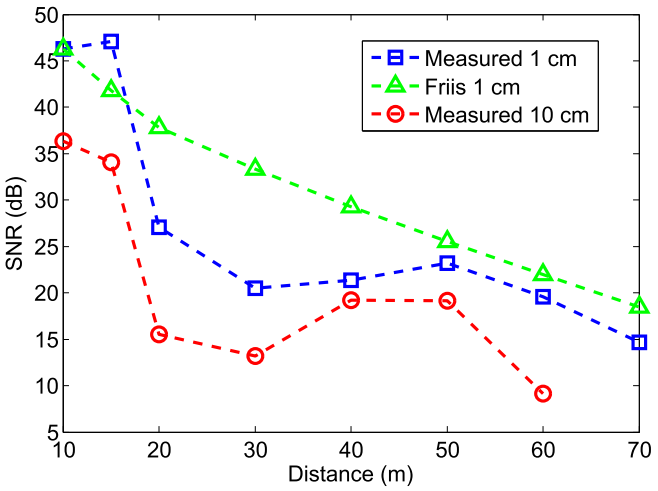

Fig. 25. Measured SNR at different distances.

TABLE I
PERFORMANCE COMPARISON BETWEEN THE EHS WITH AND WITHOUT AN RF AMPLIFIER

	With Amplifier	Without Amplifier
Max. Distance Tag-EH	80 cm	10 cm
Max. Distance Reader-Tag	>70 m	17 m

away from the EH as shown in Fig. 23. This experiment is used to evaluate the power level of the interrogating carrier at 929 MHz on the tag. The measured 929-MHz received power level by the antenna of the tag is −22.2 dBm and −16.5 dBm for topologies without and with amplifier, respectively.

The measurement setup of the entire system is shown in Fig. 24 and the EH utilized is the one with an RF amplifier. The sampling frequency is 250 kHz and the number of fast Fourier transform samples is 1024. Thus, the frequency resolution of the software defined reader is about 244 Hz. Furthermore, Nyquist theorem states that

$$f_s \geq 2B \tag{1}$$

where f_s is the sampling frequency and B is the bandwidth. By (1), the bandwidth is about 125 kHz. The channel capacity can be calculated by the Shannon equation

$$C = B\log_2(1 + \text{SNR}) \tag{2}$$

where C is the channel capacity and B is the bandwidth. Thus, by (2), the channel capacity for the system while the distance between the reader and the tag is 70 m is about 0.6 Mb/s.

As depicted in Fig. 24, three major spikes are detected by the software defined reader. The center spike is the carrier and the other two spikes which are symmetric with respect to the carrier are the backscattered signals. Since the modulation frequency is 100 kHz, the distances between the carrier and the backscattered signals are also 100 kHz. The backscattering signals are not drastically affected by the noise generated by the two-way radio. The reason is that the only significant side-band noise from radio which falls into the operating bandwidth occurs at 929 MHz. However, this is the same frequency as the carrier frequency and there would be no backscattering signals at that frequency. Both the proposed EH with and without the amplifier are measured and the maximum distances between the tag and the proposed EH and between the tag and the software defined reader are summarized in Table I. As shown in Table I, with the help of the 929-MHz carrier emitted from the proposed EH, the backscattered signal from the proposed RFID tag can be detected by the software defined reader which is located at 17 m away. Moreover, if the dc power from the proposed EH is utilized to drive the additional RF amplifier, shown in Fig. 11, and enhance the carrier emitter signals, the reading range can be extended significantly to 70 m as shown in the measurements. Furthermore, as shown in Fig. 24, the backscattered signals are 14.7 dB above the noise floor, which means a 14.7-dB signal-to-noise ratio (SNR). As the typically required SNR for detection is 3 dB, there is still a margin of 11.7 dB. According to Friis equation, this implies the reading range can be extended more than 3.8 times, i.e., more than 266 m. Similarly, as depicted in Table I, the maximum distance between the tag and the EH is also extended to 80 cm which is long enough to effectively cover all on-body backscattering sensor tags.

In order to investigate the effects of multipath and nearby clutters on the sensing range, the SNRs of the detected

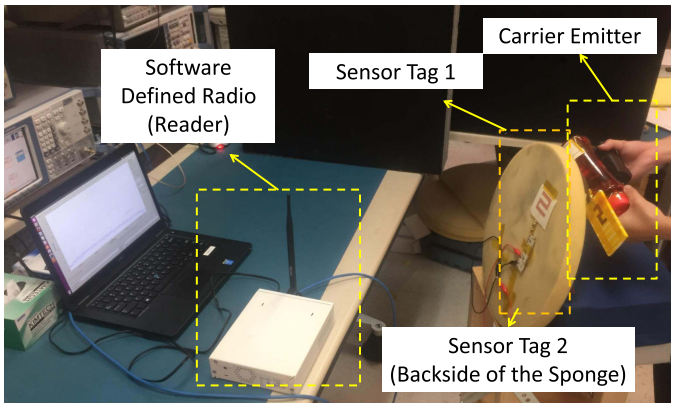

Fig. 26. Measurement setup for the multiple sensors test.

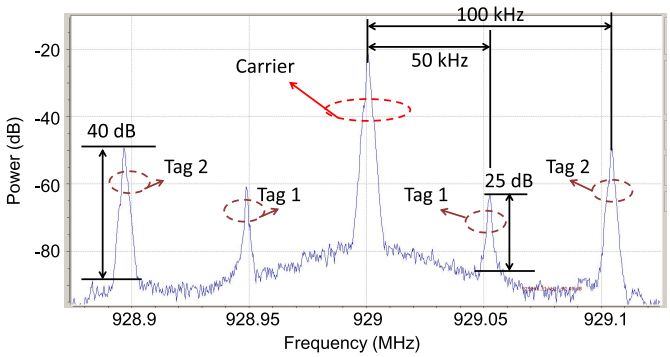

Fig. 27. Measured result for multiple sensors test.

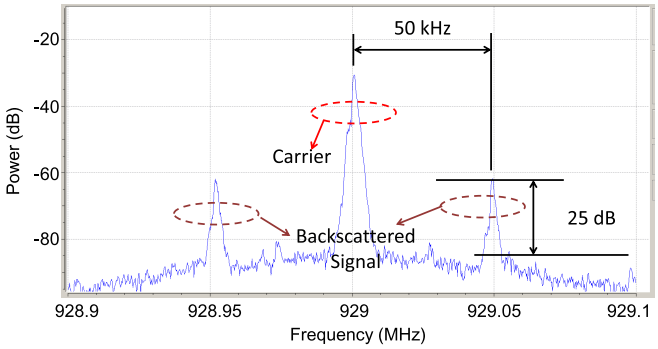

Fig. 28. Measured result for the ammonia sensor tag before exposure to ammonia.

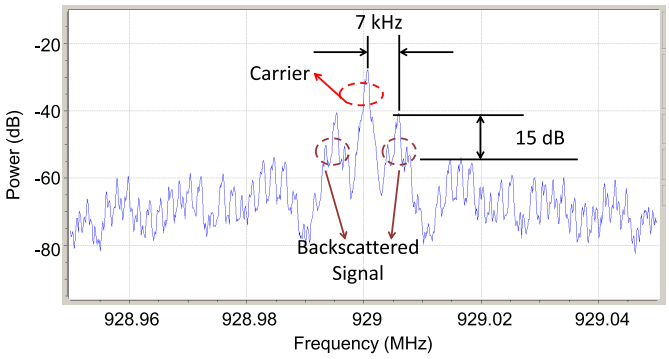

Fig. 29. Measured result for the ammonia sensor tag after exposure to ammonia.

backscattering signals were measured while varying the distance between the reader and the tag and the distance between the proposed EH and the tag. The indoor measured results are demonstrated in Fig. 25. The horizontal axis is the distance between the reader and the tag. Two different distances (1 and 10 cm) between the proposed EH and the tag were tested. Moreover, the theoretical results calculated using Friis equation are also included for comparison. As shown in Fig. 25, theoretically the SNR of the 10 cm case is 20 dB lower than 1-cm case. However, since the distance between the proposed EH and the tag is not long, near-field coupling occurs that reduces the SNR drop due to increase in distance. For the 1-cm case, the general trend is the same as the Friis equation. However, constructive interference occurs at 15 m and destructive interferences occurs at 20, 30, and 40 m. The general trend for the 10-cm case is similar to the 1-cm one. Thus, although the complex interferences due to multipath and ambient clutters cannot be accurately predicted, Friis equation can serve as a good approximation to predict the SNR at even longer distances.

B. Multiple Backscattering Tags

Since the proposed on-body WSN system typically consists of multiple sensor tags, different modulation frequencies are assigned for each sensor tag to enable simultaneous multiple sensor detection. Therefore, the experimental setup shown in Fig. 26 was used to demonstrate those multiple tags operating at different modulation frequencies which can be detected by the reader at the same time. As shown in Fig. 26, two tags are placed on the two sides of a sponge and interrogated with the carrier emitter (EH). The software defined reader is placed around 60 cm away from the tags. The measured results using the software defined reader is shown in Fig. 27. As demonstrated in Fig. 27, two tags with different modulation frequencies (50 and 100 kHz) were successfully detected simultaneously. Moreover, five spikes can be observed. The center spike is the carrier and the two symmetric spikes with 25-dB SNR which are located at 50 kHz away from the carrier are the backscattered signals from the first tag. The remaining two spikes with 40-dB SNR, which are located at 100 kHz away from the carrier are the backscattered signals from the second tag. The difference of the SNR values between the two tags is due to the fact that the distance between "ON" and "OFF" resistances on the Smith chart as shown Fig. 16 are different for two tags.

C. Ammonia Sensor

The backscattering tag that was integrated with the ammonia sensor is tested with the similar experiment setup shown in Fig. 26. The only difference is that there is only one sensor tag and the tag is exposed to ammonia gas during the measurement. The measured results of the tag before and after being exposed to ammonia gas are shown in Figs. 28 and 29, respectively. As shown in Fig. 28, the modulation frequency of the ammonia sensor tag is 50 kHz before the tag is exposed

TABLE II
COMPARISON BETWEEN THIS PAPER AND PREVIOUS RELATED WORKS

Work	Operating Frequency	RFID Type	Energy for Tag	Energy for Carrier Emitter	Reading range (m)
[21]	915 MHz	Passive	Harvested	NA	4
[22]	868 MHz	Passive	Harvested	NA	6
[23]	900 MHz	Passive	Harvested	NA	9
[24]	865 ∼870 MHz	Passive	Harvested	NA	14
[25]	34.45 GHz	Active	Battery	NA	11.5
[26]	308 MHz	Active	Battery	NA	46
[14]	867 MHz	Semi-passive + Carrier Emitter	Battery	Battery	130
This Work	929 MHz	Passive + Carrier Emitter	Harvested	Harvested	70

to the ammonia gas. The impedance of the ammonia sensor is increased after the ammonia gas exposure effectively decreases the modulation frequency to 7 kHz as shown in Fig. 29. Due to the frequency change of the backscattered signals, the ammonia gas can be easily detected ("red/green detection") by processing the received data.

D. Comparison

The comparison between this paper and previous related research efforts are shown in Table II. As demonstrated in Table II, reading ranges only up to around 10 m can be achieved by purely passive RFID tags. The reading ranges of the active RFID tags are larger than purely passive ones. For example, 46-m reading range is achieved in [26]. In [14], a very long (130 m) reading range is achieved utilizing semipassive backscattering tags and carrier emitters. However, batteries are used in both tags and carrier emitters. The reading range of this paper is much longer compared with other previous works listed in except Table II [14]. Compared with [14], the energy harvesting techniques utilized in this paper support all energy requirements and enable a fully energy autonomous system, thus leading to much lower maintenance costs.

VII. CONCLUSION

This paper proposed a novel on-body WSN system. The system is fully energy autonomous and the reading ranges of the sensor tags are drastically enhanced utilizing a wearable and flexible EH harvesting energy from a two-way talk radio. For the first time reported, the proposed EH utilizes not only the dc power to drive an RF power amplifier but also the second harmonic to build a mobile carrier emitter to significantly enhance configuration reading ranges of on-body sensing capable RFID tags. The output dc and 929-MHz power is 16.5 and 13 dBm, respectively, while the 34.3-dBm transmitting power two-way talk radio is 9 cm away. The 929-MHz antenna is designed along with an AMC structure to reduce the interference of the human body. Moreover, the custom 3-D printed flexible substrate is applied to the AMC design to eliminate the limitation of the substrate thickness of off-the-shelf materials. The inkjet printing masking technique is also applied to the fabrication of the EH on nearly every flexible substrate to reduce the cost. A custom backscattering tag which operates with −5 dBm of input power was realized and an ammonia sensor was integrated into the backscattering tag to demonstrate the inherent advantage of the proposed system to IoT applications requiring multiple wireless sensors and tags. The reading range was extended to more than 70 m by integrating the RF amplifier which is powered by harvester energy. Moreover, multiple experiments are performed to demonstrate multiple tag interrogation and gas detection capabilities.

REFERENCES

[1] L. Atzori, A. Iera, and G. Morabito, "The Internet of Things: A survey," *Comput. Netw.*, vol. 54, no. 15, pp. 2787–2805, Oct. 2010.
[2] A. Ö. Ercan, O. Sunay, and I. F. Akyildiz, "RF energy harvesting and transfer for spectrum sharing cellular IoT communications in 5G systems," *IEEE Trans. Mobile Comput.*, to be published.
[3] M. Pinuela, P. D. Mitcheson, and S. Lucyszyn, "Ambient RF energy harvesting in urban and semi-urban environments," *IEEE Trans. Microw. Theory Techn.*, vol. 61, no. 7, pp. 2715–2726, Jul. 2013.
[4] R. J. Vyas, B. B. Cook, Y. Kawahara, and M. M. Tentzeris, "E-WEHP: A batteryless embedded sensor-platform wirelessly powered from ambient digital-TV signals," *IEEE Trans. Microw. Theory Techn.*, vol. 61, no. 6, pp. 2491–2505, Jun. 2013.
[5] J. A. Paradiso and T. Starner, "Energy scavenging for mobile and wireless electronics," *IEEE Pervasive Comput.*, vol. 4, no. 1, pp. 18–27, Jan./Mar. 2005.
[6] M. Arrawatia, M. S. Baghini, and G. Kumar, "Broadband bent triangular omnidirectional antenna for RF energy harvesting," *IEEE Antennas Wireless Propag. Lett.*, vol. 15, pp. 36–39, Apr. 2016.
[7] C. Song *et al.*, "A novel six-band dual CP rectenna using improved impedance matching technique for ambient RF energy harvesting," *IEEE Trans. Antennas Propag.*, vol. 64, no. 7, pp. 3160–3171, Jul. 2016.
[8] S. Kim *et al.*, "Ambient RF energy-harvesting technologies for self-sustainable standalone wireless sensor platforms," *Proc. IEEE*, vol. 102, no. 11, pp. 1649–1666, Nov. 2014.
[9] J. Bito, J. G. Hester, and M. M. Tentzeris, "Ambient RF energy harvesting from a two-way talk radio for flexible wearable wireless sensor devices utilizing inkjet printing technologies," *IEEE Trans. Microw. Theory Techn.*, vol. 63, no. 12, pp. 4533–4543, Dec. 2015.
[10] C. R. Valenta and G. D. Durgin, "Harvesting wireless power: Survey of energy-harvester conversion efficiency in far-field, wireless power transfer systems," *IEEE Microw. Mag.*, vol. 15, no. 4, pp. 108–120, Jun. 2014.
[11] D. De Donno, L. Catarinucci, and L. Tarricone, "An UHF RFID energy-harvesting system enhanced by a DC–DC charge pump in silicon-on-insulator technology," *IEEE Microw. Wireless Compon. Lett.*, vol. 23, no. 6, pp. 315–317, Jun. 2013.
[12] X. Lu, P. Wang, D. Niyato, D. I. Kim, and Z. Han, "Wireless networks with RF energy harvesting: A contemporary survey," *IEEE Commun. Surveys Tuts.*, vol. 17, no. 2, pp. 757–789, 2nd Quart., 2015.
[13] J. Bito *et al.*, "Inkjet-/3D-/4D-printed autonomous wearable RF modules for biomonitoring, positioning and sensing applications," *Proc. SPIE*, vol. 10194, p. 101940Z, May 2017.
[14] J. Kimionis, A. Bletsas, and J. N. Sahalos, "Increased range bistatic scatter radio," *IEEE Trans. Commun.*, vol. 62, no. 3, pp. 1091–1104, Mar. 2014.

[15] T.-H. Lin, J. Bito, J. G. Hester, J. Kimionis, R. A. Bahr, and M. M. Tentzeris, "Ambient energy harvesting from two-way talk radio for on-body autonomous wireless sensing network using inkjet and 3D printing," in *IEEE MTT-S Int. Microw. Symp. Dig.*, Jun. 2017, pp. 1034–1037.
[16] A. P. Feresidis, G. Goussetis, S. Wang, and J. C. Vardaxoglou, "Artificial magnetic conductor surfaces and their application to low-profile high-gain planar antennas," *IEEE Trans. Antennas Propag.*, vol. 53, no. 1, pp. 209–215, Jan. 2005.
[17] R. Bahr *et al.*, "RF characterization of 3D printed flexible materials—NinjaFlex filaments," in *Proc. Eur. Microw. Conf. (EuMC)*, Sep. 2015, pp. 742–745.
[18] J. Kimionis and M. M. Tentzeris, "Pulse shaping: The missing piece of backscatter radio and RFID," *IEEE Trans. Microw. Theory Techn.*, vol. 64, no. 12, pp. 4774–4788, Dec. 2016.
[19] E. Kampianakis, J. Kimionis, K. Tountas, C. Konstantopoulos, E. Koutroulis, and A. Bletsas, "Wireless environmental sensor networking with analog scatter radio and timer principles," *IEEE Sensors J.*, vol. 14, no. 10, pp. 3365–3376, Oct. 2014.
[20] E. Bekyarova *et al.*, "Chemically functionalized single-walled carbon nanotubes as ammonia sensors," *J. Phys. Chem. B*, vol. 108, no. 51, pp. 19717–19720, Oct. 2004.
[21] A. A. Kutty, T. Björninen, L. Sydänheimo, and L. Ukkonen, "A novel carbon nanotube loaded passive UHF RFID sensor tag with built-in reference for wireless gas sensing," in *IEEE MTT-S Int. Microw. Symp. Dig.*, May 2016, pp. 1–4.
[22] G. A. Vera, S. D. Nawale, Y. Duroc, and S. Tedjini, "Read range enhancement by harmonic energy harvesting in passive UHF RFID," *IEEE Microw. Wireless Compon. Lett.*, vol. 25, no. 9, pp. 627–629, Sep. 2015.
[23] J.-W. Lee and B. Lee, "A long-range UHF-band passive RFID tag IC based on high-Q design approach," *IEEE Trans. Ind. Electron.*, vol. 56, no. 7, pp. 2308–2316, Jul. 2009.
[24] A. Popov, S. Dudnikov, and A. Mikhaylov, "Passive UHF RFID tag with increased read range," in *Proc. 38th Eur. Microw. Conf.*, Oct. 2008, pp. 1106–1108.
[25] A. Strobel, C. Carlowitz, R. Wolf, F. Ellinger, and M. Vossiek, "A millimeter-wave low-power active backscatter tag for FMCW radar systems," *IEEE Trans. Microw. Theory Techn.*, vol. 61, no. 5, pp. 1964–1972, May 2013.
[26] L. M. Ni, Y. Liu, Y. C. Lau, and A. P. Patil, "LANDMARC: Indoor location sensing using active RFID," in *Proc. 1st IEEE PerCom*, Mar. 2003, pp. 407–415.

Tong-Hong Lin received the B.S.E.E. and M.S. degrees from National Taiwan University, Taipei, Taiwan, in 2011 and 2013, respectively. He is currently pursuing the Ph.D. degree in electrical and computer engineering and M.S. degree in computational science and engineering at the Georgia Institute of Technology, Atlanta, GA, USA.

He is currently a Research Assistant with the ATHENA Group, Georgia Institute of Technology. His current research interests include additive manufacturing techniques such as inkjet printing and 3-D printing, wearable and flexible electronics, RF energy harvesting systems, packaging design, wireless power transfer systems, and wireless sensing networks.

Jo Bito (S'13) received the B.S. degree in electrical and electronic engineering from Okayama University, Okayama, Japan in 2013, and the M.S. degree and Ph.D. degree in electrical and computer engineering from the Georgia Institute of Technology, Atlanta, GA, USA in 2016 and 2017, respectively.

From 2010 to 2011, he joined the international programs in engineering (IPENG) and studied at the University of Illinois Urbana–Champaign, Champaign, IL, USA. He is currently a Research Engineer with Texas Instrument Incorporated, Dallas TX, USA. His research interests include the application of inkjet printing technology for flexible and wearable electronics, RF energy harvesting, wireless power transfer systems, millimeter-wave electronics, and semiconductor packaging.

Dr. Bito was a recipient of the Japan Student Services Organization (JASSO) long term scholarship from 2013.

Jimmy G. D. Hester (GS'14–M'17) received the bachelor's degree from INP Toulouse, Toulouse, France, in 2012, the M.S. degree in electrical and signal processing engineering (with a major in radio frequency electronics) from ENSEEIHT, Toulouse, in 2014, and the M.S. degree in electrical and computer engineering from the Georgia Institute of Technology, Atlanta, GA, USA, in 2014, where he is currently pursuing the Ph.D. degree in electrical and computer engineering.

He is currently a Research Assistant with the ATHENA Group, Georgia Institute of Technology. Recently, he has been developing solutions for the use of carbon nanomaterials, as well as optimized RF structures toward the implementation of inkjet-printed flexible low-cost ubiquitous gas sensors for Internet of Things and smart skin applications. He was involved in the entire development process, from the development of inkjet inks, improvement of fabrication methods, sensor component design, high-frequency characterization, environmental testing to the design, simulation, fabrication of the RF system embedding the sensor, and the development of wireless reading and data processing schemes. His current research interests include the interface between radio frequency and mm-wave engineering and material science in the form of flexible electronics technologies and nanotechnologies.

Mr. Hester was a recipient of the 2015 NT4D Student Award, the Second Place Best Poster Award of the 2017 IEEE Futurecar Conference, the Third Place Best Poster Award of the 2017 Flex Conference, and a Honorable Mention Award as Finalist of the 2017 IEEE MTT-S IMS Student Paper Competition.

John Kimionis (S'10–M'17) received the Diploma and M.Sc. degrees in electronic and computer engineering from the Technical University of Crete, Chania, Greece, in 2011 and 2013, respectively. He is currently pursuing the Ph.D. degree at the School of Electrical and Computer Engineering, Georgia Institute of Technology, Atlanta, GA, USA.

He was a Research Assistant with the ATHENA Group, Georgia Institute of Technology. In 2017, he was a Research Intern with Nokia Bell Labs, Murray Hill, NJ, USA. His current research interests include spectral-efficient and energy-efficient backscatter radio and RFID, software-defined radio for sensor networks, RF front-end design for wireless sensors, and additive manufacturing techniques (inkjet- and 3-D-printed electronics).

Mr. Kimionis was a recipient of the Fellowship Award for his undergraduate and graduate studies and has been a Texas Instruments Scholar for his mentoring service for the Opportunity Research Scholars Program of the Georgia Institute of Technology. He was a recipient of the IEEE Student Travel Grant and the First Best Student Paper Award of the IEEE International Conference on RFID-TA 2014, Tampere, Finland, the Second Best Student Paper Award of the IEEE International Conference on RFID-Technologies and Applications 2011, Sitges, Barcelona, Spain, and the Third Bell Labs Prize Award 2016 for game-changing technologies on printed electronics and low-cost communications. He has been a member of the IEEE Microwave Theory and Techniques Society and the IEEE Communications Society and is a Board member of the IEEE MTT-24 RFID Technologies Committee. He currently serves as the Finance Chair of the IEEE International Conference on RFID 2018.

Ryan A. Bahr (GS'14) received the B.S. degree (*summa cum laude*) (with a focus on RF engineering) and M.S. degree (with a focus on electromagnetics and a minor in computer science) from the Georgia Institute of Technology, Atlanta, GA, USA, in 2013 and 2015, respectively.

He is currently a Research Assistant with the ATHENA Research Laboratory, Georgia Institute of Technology, where he focuses on the development of 3-D electromagnetic designs utilizing additive manufacturing. He designs complex electromagnetic structures with additive manufacturing utilizing technologies such as fused deposition modeling, stereolithography, and inkjet printing. He is involved in mathematically inspired structures, inkjet printing of flexible electronics, and the utilization of additive manufacturing for RF packaging and mm-wave electronics.

Mr. Bahr was the recipient of the Best Student Poster Award of Gomac Tech 2016 for additively manufactured flexible and origami-reconfigurable RF sensors.

Manos M. Tentzeris (S'89–M'92–SM'03–F'10) received the Diploma degree (*magna cum laude*) in electrical and computer engineering from the National Technical University of Athens, Athens, Greece, and the M.S. and Ph.D. degrees in electrical engineering and computer science from the University of Michigan, Ann Arbor, MI, USA.

He is currently Ken Byers Professor in flexible electronics with the School of Electrical and Computer Engineering, Georgia Institute of Technology, Atlanta, GA, USA, where he heads the ATHENA Research Group (20 researchers). He has served as the Head of the GT-ECE Electromagnetics Technical Interest Group, as the Georgia Electronic Design Center Associate Director of RFID/Sensors research, as the Georgia Institute of Technology NSF-Packaging Research Center Associate Director of RF Research, and as the RF Alliance Leader. He has helped develop academic programs in 3-D/inkjet-printed RF electronics and modules, flexible electronics, origami and morphing electromagnetics, highly integrated/multilayer packaging for RF and wireless applications using ceramic and organic flexible materials, paper-based RFID's and sensors, wireless sensors and biosensors, wearable electronics, "Green" electronics, energy harvesting and wireless power transfer, nanotechnology applications in RF, microwave MEMs, and SOP-integrated (UWB, multiband, mmW, and conformal) antennas. He has authored more than 650 papers in refereed journals and conference proceedings, 5 books, and 25 book chapters. He was a Visiting Professor with the Technical University of Munich, Munich, Germany, in 2002, with GTRI-Ireland, Athlone, Ireland, in 2009, and with LAAS-CNRS, Toulouse, France, in 2010.

Dr. Tentzeris was a recipient/co-recipient of the 2017 Georgia Institute of Technology Outstanding Achievement in Research Program Development Award, the 2016 Bell Labs Award Competition 3rd Prize, the 2015 IET Microwaves, Antennas, and Propagation Premium Award, the 2014 Georgia Institute of Technology ECE Distinguished Faculty Achievement Award, the 2014 IEEE RFID-TA Best Student Paper Award, the 2013 IET Microwaves, Antennas and Propagation Premium Award, the 2012 FiDiPro Award in Finland, the iCMG Architecture Award of Excellence, the 2010 IEEE Antennas and Propagation Society Piergiorgio L. E. Uslenghi Letters Prize Paper Award, the 2011 International Workshop on Structural Health Monitoring Best Student Paper Award, the 2010 Georgia Institute of Technology Senior Faculty Outstanding Undergraduate Research Mentor Award, the 2009 IEEE TRANSACTIONS ON COMPONENTS AND PACKAGING TECHNOLOGIES Best Paper Award, the 2009 E. T. S. Walton Award from the Irish Science Foundation, the 2007 IEEE AP-S Symposium Best Student Paper Award, the 2007 IEEE MTT-S IMS Third Best Student Paper Award, the 2007 ISAP 2007 Poster Presentation Award, the 2006 IEEE MTT-S Outstanding Young Engineer Award, the 2006 Asia–Pacific Microwave Conference Award, the 2004 IEEE TRANSACTIONS ON ADVANCED PACKAGING Commendable Paper Award, the 2003 NASA Godfrey "Art" Anzic Collaborative Distinguished Publication Award, the 2003 IBC International Educator of the Year Award, the 2003 IEEE CPMT Outstanding Young Engineer Award, the 2002 International Conference on Microwave and Millimeter-Wave Technology Best Paper Award (Beijing, China), the 2002 Georgia Institute of Technology–ECE Outstanding Junior Faculty Award, the 2001 ACES Conference Best Paper Award, the 2000 NSF CAREER Award, and the 1997 Best Paper Award of the International Hybrid Microelectronics and Packaging Society. He was the TPC Chair of the IEEE MTT-S IMS 2008 Symposium and the Chair of the 2005 IEEE CEM-TD Workshop. He is the Vice-Chair of the RF Technical Committee (TC16) of the IEEE CPMT Society. He is the Founder and Chair of the RFID Technical Committee (TC24) of the IEEE MTT-S and the Secretary/Treasurer of the IEEE C-RFID. He is an Associate Editor of the IEEE TRANSACTIONS ON MICROWAVE THEORY AND TECHNIQUES, the IEEE TRANSACTIONS ON ADVANCED PACKAGING, and the *International Journal on Antennas and Propagation*. He has given more than 100 invited talks to various universities and companies all over the world. He is a member of the URSI-Commission D and the MTT-15 Committee, an Associate Member of EuMA, a Fellow of the Electromagnetic Academy, and a member of the Technical Chamber of Greece. He served as one of the IEEE MTT-S Distinguished Microwave Lecturers from 2010 to 2012 and is one of the IEEE CRFID Distinguished Lecturers.